X-Ray-Controlled Generation of Peroxynitrite Based on Nanosized LiLuF$_4$:Ce^{3+} Scintillators and their Applications for Radiosensitization

Zhen Du, Xiao Zhang, Zhao Guo, Jiani Xie, Xinghua Dong, Shuang Zhu, Jiangfeng Du, Zhanjun Gu,* and Yuliang Zhao

Peroxynitrite (ONOO$^-$), the reaction product derived from nitric oxide (NO) and superoxide (O$_2^{-\bullet}$), is a potent oxidizing and nitrating agent that modulates complex biological processes and promotes cell death. Therefore, it can be expected that the overproduction of ONOO$^-$ in tumors can be an efficient approach in cancer therapy. Herein, a multifunctional X-ray-controlled ONOO$^-$ generation platform based on scintillating nanoparticles (SCNPs) and UV-responsive NO donors Roussin's black salt is reported, and consequently the mechanism of their application in enhanced therapeutic efficacy of radiotherapy is illustrated. Attributed to the radioluminescence and high X-ray-absorbing property of SCNPs, the nanocomposite can produce NO and O$_2^{-\bullet}$ simultaneously when excited by X-ray irradiation. Such simultaneous release of NO and O$_2^{-\bullet}$ ensures the efficient X-ray-controlled generation of ONOO$^-$ in tumors. Meanwhile, the application of X-rays as the excitation source can achieve better penetration depth and induce radiotherapy in this nanotherapeutic platform. It is found that the X-ray-controlled ONOO$^-$-generation platform can efficiently improve the radiotherapy efficiency via directly damaging DNA, downregulating the expression of the DNA-repair enzyme, and overcoming the hypoxia-associated resistance in radiotherapy. Therefore, this SCNP-based platform may provide a new combinatorial strategy of ONOO$^-$ and radiotherapy to improve cancer treatment.

Peroxynitrite (ONOO$^-$) is considered to be a powerful oxidizing and nitrating agent, which can be endogenously generated by the diffusion-limited reaction of nitric oxide (NO) with superoxide (O$_2^{-\bullet}$).[1] It is verified that neither NO nor O$_2^{-\bullet}$ is particularly toxic in vivo, because they can be rapidly scavenged by oxyhemoglobin and superoxide dismutase (SOD), respectively.[2] However, in the presence of NO and O$_2^{-\bullet}$, ONOO$^-$ can be formed because their reaction is extremely fast so that NO can outcompete SOD for O$_2^{-\bullet}$.[3] The generated ONOO$^-$ appear to be far more toxic than most free radicals, including hydroxyl radical (•OH).[4] Such toxicity is attributed to its peculiar properties involving direct oxidation as well as radical-mediated nitration reactions, which allows ONOO$^-$ to regulate signal transduction pathways by altering the structure of various proteins, induce DNA strand breaks, destroy membrane structure by lipid peroxidation, directly injure the mitochondria, and promote cell death.[5] Therefore, it is expected that the overproduction of ONOO$^-$ in tumors can be an efficient approach in cancer therapy.

Due to the transitory lifetime and short diffusion distance of NO and O$_2^{-\bullet}$, their simultaneous production in the same region becomes a big challenge for the efficient generation of ONOO$^-$. In order to solve such problem, the controllable generation of these reactive species using exogenously stimulus-responsive nanotherapeutic platform may be the most effective solution.[6] Among all external stimulation, light as the trigger can precisely fix a position on the tumor with high spatiotemporal resolution as well as fewer side effects. In order to realize the efficient generation of ONOO$^-$, simultaneous generation of NO and O$_2^{-\bullet}$ at the same place is

Dr. Z. Du, Dr. X. Zhang, Dr. Z. Guo, Dr. J. Xie, Dr. X. Dong, S. Zhu, Prof. Z. Gu, Prof. Y. Zhao
CAS Key Laboratory for Biomedical Effects of Nanomaterials and Nanosafety
Institute of High Energy Physics
Chinese Academy of Sciences
Beijing 100049, China
E-mail: zjgu@ihep.ac.cn

Dr. Z. Du, Dr. X. Zhang, Dr. Z. Guo, Dr. J. Xie, Dr. X. Dong, Prof. Z. Gu, Prof. Y. Zhao
College of Materials Science and Optoelectronic Technology
University of Chinese Academy of Sciences
Beijing 100049, China

Dr. J. Du
Department of Medical Imaging
First Hospital of Shanxi Medical University
Taiyuan, Shanxi 030001, China

Prof. Y. Zhao
CAS Center for Excellence in Nanoscience
National Center for Nanoscience and Technology of China
Chinese Academy of Sciences
Beijing 100190, China

**ADVANCED
SCIENCE NEWS**

www.advancedsciencenews.com

**ADVANCED
MATERIALS**

www.advmat.de

needed to be accomplished. Recently, previous studies have reported different kinds of strategies to achieve controllable generation of NO triggered by UV, vis, and even NIR light.[7] However, the poor tissue penetration of UV and vis as well as the low efficiency of NIR light significantly limits their effective applications. To overcome these problems, scintillating nanoparticles (SCNPs) were introduced as the energy transducers to convert the high-penetrating X-ray into UV–vis lights in situ,[8] and further activate the surrounding photoactive donors to release NO. In this design, X-ray is introduced as an ideal excitation source because it has great penetration in the human body.[9] More importantly, many reactive oxygen species (ROS) including $O_2^{-\bullet}$ are formed by the radiolysis under X-ray irradiation exposure leading to the X-ray-induced $O_2^{-\bullet}$ generation.[10] Additionally, nanoparticles containing high-Z element can promote the production of $O_2^{-\bullet}$ in radiotherapy because of its high X-ray absorption ability and strong reaction with surround oxygen and water.[11] As a consequence, using X-ray as the energy source and high-Z SCNPs as the energy mediators can achieve the goal of producing NO and $O_2^{-\bullet}$ simultaneously and further generating powerful $ONOO^-$ for cancer therapy.

In this work, we report a theranostic SCNPs system containing Ce-doped $LiLuF_4$ and Roussin's black salt (RBS) for the on-demand generation of $ONOO^-$ under X-ray irradiation. On the one hand, the Ce-doped $LiLuF_4$ can act as radiosensitizers for enhancing the yield of ROS including $O_2^{-\bullet}$ under X-ray irradiation. On the other hand, Ce-doped $LiLuF_4$ could convert X-ray into UV light to activate the photoactive RBS to release NO. Such X-ray-controlled simultaneous release of NO and $O_2^{-\bullet}$ ensures the efficient generation of $ONOO^-$. Benefited from the biomedical effect of $ONOO^-$, the radiotherapy sensitization ability of the nanocomposite was evaluated in vitro and in vivo. We found that the released $ONOO^-$ could improve radiotherapy efficiency by directly damaging DNA and inhibiting the expression of the DNA-repair enzyme, leading to the augment of DNA damage and inhibition of tumor growth. In addition, NO as well as $ONOO^-$ can function as powerful vasodilators and hypoxia inducible factor-1α (HIF-1α) inhibitors, so as to overcome the hypoxia-associated radioresistance.[12] Furthermore, in consideration of the strong X-ray attenuation, the as-synthesized nanoparticles can be applied as a computed tomography (CT) contrast agent, which may offer an additional method for diagnostic application. Our work may provide a new strategy for the controllable generation of $ONOO^-$ under X-ray irradiation and efficient radiotherapy sensitization in cancer treatment.

The synthetic route of the nanocomposites and their applications of X-ray-controlled $ONOO^-$ generation for the on-demand cancer radiotherapy are illustrated in **Scheme 1**. The SCNPs were synthesized according to the literature procedure with slight modification.[13] Transmission electron microscope (TEM) and scanning electron microscope images showed that the morphology of the as-synthesized $LiLuF_4$:Ce^{3+} nanoparticles was roughly rhomboid, with an average diameter of about 70 nm (**Figure 1**a and Figure S1, Supporting Information). The X-ray diffraction (XRD) patterns were used to confirm the crystal structure of SCNPs. As shown in Figure 1b, the XRD pattern of the SCNPs agreed well with the standard pattern of tetragonal-phase $LiLuF_4$ (JCPDS No. 027-1251). The radioluminescence spectrum of SCNPs exhibited the emission bands at

306 and 326 nm, which were attributed to the transitions from the lowest 5d level to the $^2F_{5/2}$ and $^2F_{7/2}$ levels of the $4f^1$ configuration in Ce^{3+}, respectively.[14] Additionally, the concentration of Ce^{3+} ions in the SCNPs was adjusted to 2% in order to obtain the most efficient radioluminescence (Figure 1c). Next, to render the as-synthesized SCNPs hydrophilic and biocompatible, the oleic acid ligands on their surface were removed by acid treatment.[15] The successful removal of the surface oleic acid was confirmed by zeta potential and Fourier transform infrared (FT-IR) spectra (Figure 1d,e). Due to the removal of surface ligands, the Lu^{3+} ions were exposed on the surface of the SCNPs, resulting in a positive zeta potential + 31.6 mV (Figure 1d). As a result, the ligand-free SCNPs are enabled to provide the positive domains for direct conjugation in aqueous solution with electronegative hydrophilic and biocompatible molecules for various bioapplications. Many studies have shown that tocopheryl polyethylene glycol 1000 succinate (TPGS), a widely applied food and drug additive, can be conjugated on the surface of nanoparticles for improving the biocompatibility and overcoming multidrug resistance in cancer therapy.[16] Therefore, we use TPGS for the further functionalization of the ligand-free SCNPs through electrostatic attraction (T-SCNPs). After conjugation, the zeta potential of the SCNPs changed from + 31.6 to + 14.4 mV. The obtained T-SCNPs showed good dispersibility in aqueous solutions (Figure 1d) and good chemical stability for more than 5 d (Figure S3, Supporting Information). Next, we chose RBS as the photoactive NO donor to produce NO under X-ray stimulation.[17] As shown in Figure 1f, the emission of SCNPs at 290–363 nm matched well with the absorption spectrum of RBS, ensuring the high-energy transfer efficiency from X-ray-induced photons to RBS molecules for generating NO. The RBS was loaded on the surface of T-SCNPs through the electrostatic interaction, and the obtained RBS-loaded SCNPs (RBS-T-SCNPs) showed a negative zeta potential of –8.4 mV (Figure 1d). The loading capacity calculated from the UV–vis absorption standard curve was proved to be about 0.11 mmol g^{-1} (6 w/w%; Figure 1g). After absorbing RBS on the surface of the T-SCNPs, an obvious fluorescence quenching was observed, indicating the efficient energy transfer from the SCNPs (donor) to RBS (acceptor; Figure 1f). The RBS-T-SCNPs were well dispersed in phosphate buffer saline (PBS) solution (50 µg mL^{-1}) to acquire the brown suspension. After centrifugation, colorless supernatant and brown precipitate were obtained, illustrating the combination of RBS and T-SCNPs (Figure 1h). The UV–vis absorption spectra also verified the success of RBS loading (Figure 1i). Additionally, less than 5% of the RBS was detached from the T-SCNPs after stirring in a physiological solution for 24 h, indicating the high stability of RBS-T-SCNPs for biomedical applications (Figure S6, Supporting Information).

According to our design, the key factor for the generation of $ONOO^-$ is to produce NO and $O_2^{-\bullet}$ simultaneously based on the as-prepared RBS-T-SCNPs. The measurements of X-ray-controlled $O_2^{-\bullet}$, NO and $ONOO^-$ generation were conducted, respectively. First, the production of $O_2^{-\bullet}$ was monitored by using the nitro blue tetrazolium (NBT), which could specifically react with $O_2^{-\bullet}$ and exhibits a maximum absorbance at 260 nm.[18] As demonstrated in **Figure 2**a, the absorbance of NBT was obviously reduced in both X-ray irradiation groups, especially in T-SCNPs + X-ray group, indicating a high
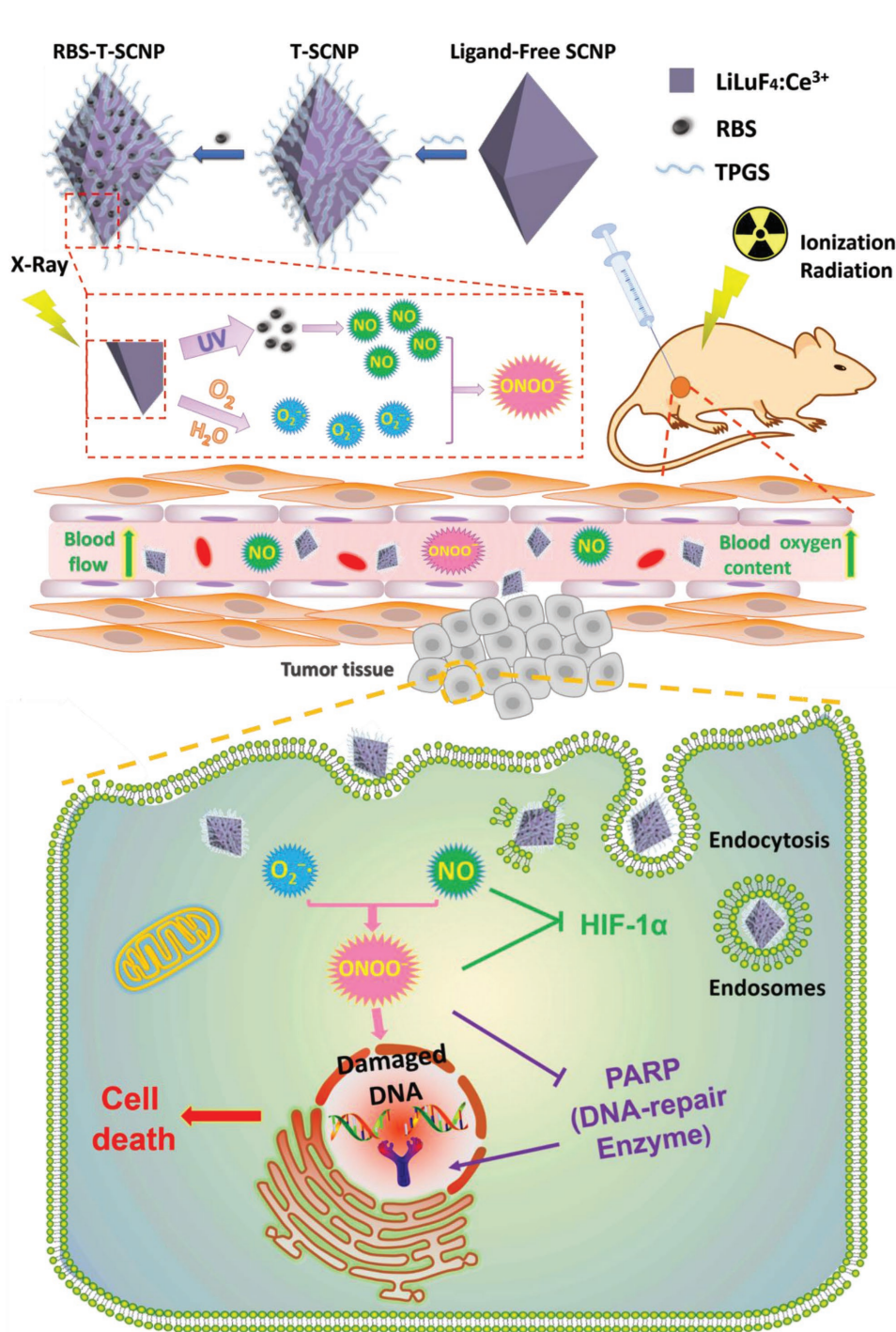
Scheme 1. Schematic illustration of the synthetic route to RBS-T-SCNPs and the X-ray-controlled ONOO⁻ generation for the on-demand cancer radiotherapy.

production of the $O_2^{-\bullet}$ by T-SCNPs under X-ray irradiation. Many research have proved that high-Z nanoparticles could increase the generation of ROS including $O_2^{-\bullet}$ in radiotherapy by the strong X-ray attenuation.[11a,b] For instance, Misawa et al. reported that Au nanoparticles in water could lead to a 7.68-fold increase of $O_2^{-\bullet}$ upon X-rays irradiation.[19] In our research, SCNPs have the ability to enhance $O_2^{-\bullet}$ in radiotherapy too, and after the loading of RBS, the RBS-T-SCNPs have the ability

to produce NO. The detection of NO was carried out using a commercial NO electrode (World Precision Instruments, Inc.). As shown in Figure 2b, the NO release curve exhibited an "on/off" feature following the absence or presence of X-ray irradiation. Besides, the total accumulation of NO along with time under different X-ray doses irradiation was measured (Figure S7, Supporting Information). The speed rate of NO generation in the first 4 min could be calculated as 0.053 nmol s⁻¹
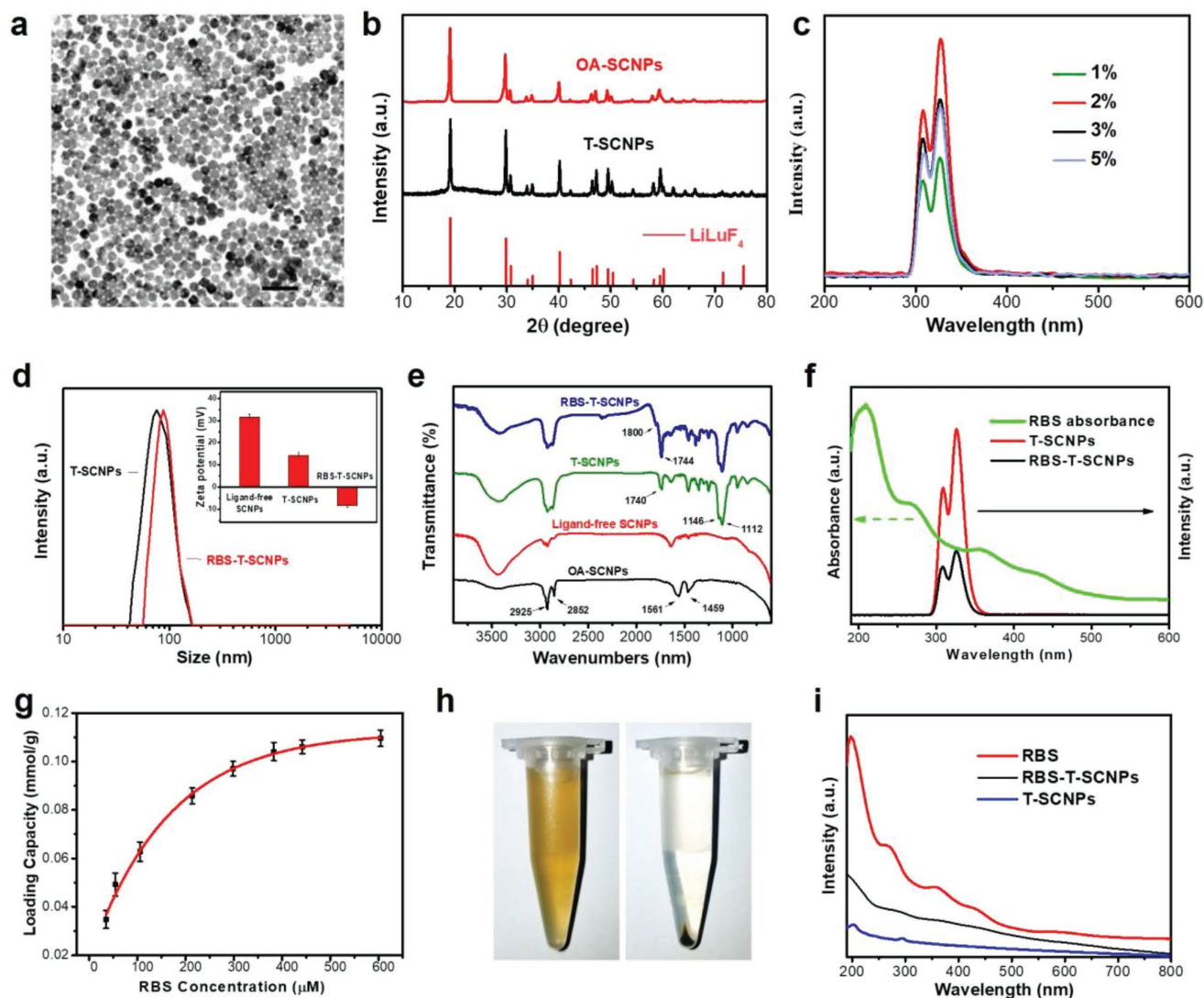
ADVANCED
SCIENCE NEWS
www.advancedsciencenews.com

ADVANCED
MATERIALS
www.advmat.de

Figure 1. Synthesis and characterization of the SCNPs. a) TEM image of LiLuF$_4$:Ce^{3+} nanoparticles. b) XRD patterns of the SCNPs. c) The radioluminescence of LiLuF$_4$:Ce^{3+} with different Ce^{3+}-doping concentrations. d) Size distribution of the SCNPs from DLS analysis. Inset: zeta potential of the SCNPs. e) The FT-IR spectra of OA-SCNPs (black), ligand-free SCNPs (red), T-SCNPs (green), and RBS-T-SCNPs (blue), respectively. f) The UV–vis absorption of free RBS (dashed line) and the radioluminescence of T-SCNPs (red) and RBS-T-SCNPs (black). g) Concentration-dependent RBS loading with a saturated capacity of 0.11 mmol g^{-1} (6 w/w%). The error bars represent standard deviation for $n = 3$. h) Photographs of RBS-T-SCNPs aqueous dispersion before (left) and after (right) centrifugation. i) UV–vis absorption spectra of RBS, T-SCNPs, and RBS-T-SCNPs, respectively.

(2 mg mL^{-1} of RBS-T-SCNPs in 10 mL of PBS solution, 50 kV, 75 µA, 100 Sv h^{-1}; Figure S8, Supporting Information). These results verified that the RBS-T-SCNPs could efficiently release NO upon X-ray irradiation. Meanwhile, a positive correlation between the amount of released NO and X-ray doses was established, which was of great importance in further applications. Based on the results of O$_2^{-\bullet}$ and NO detection, the generation of ONOO$^-$ was further measured by L-Tyrosine (L-tyr), which could be oxidized by ONOO$^-$ in the presence of CO$_2$. The oxidized dimerization of tyrosine (Dityr) was measured at excitation wavelength of 313 nm and emission wavelength of 406 nm.[5b] As shown in Figure 2c, the fluorescence signal of L-Tyrosine showed no visible difference between the control and RBS-T-SCNPs groups. However, the fluorescence intensity at 406 nm became quite strong in the RBS-T-SCNPs + X-ray

group, indicating the effective generation of ONOO$^-$ from RBS-T-SCNPs under X-ray irradiation. These results suggested that the RBS-T-SCNPs could produce NO and O$_2^{-\bullet}$ simultaneously and further generate ONOO$^-$ upon X-ray irradiation in an on-demand manner.

In addition to the measurements in physiological solution, the corresponding experiments were also performed in human nonsmall cell carcinoma A549 cells. All the detailed parameters of the in vitro radiotherapy experiments are shown in Table S1 in the Supporting Information. The cellular O$_2^{-\bullet}$ was detected by a commercial superoxide fluorescence indicator, dihydroethidium (DHE). As shown in Figure 2d, the fluorescence intensities of DHE in all the X-ray treated groups were significantly stronger than all the unirradiated groups. The quantified data from flow cytometry indicated that a large amount of O$_2^{-\bullet}$ was generated
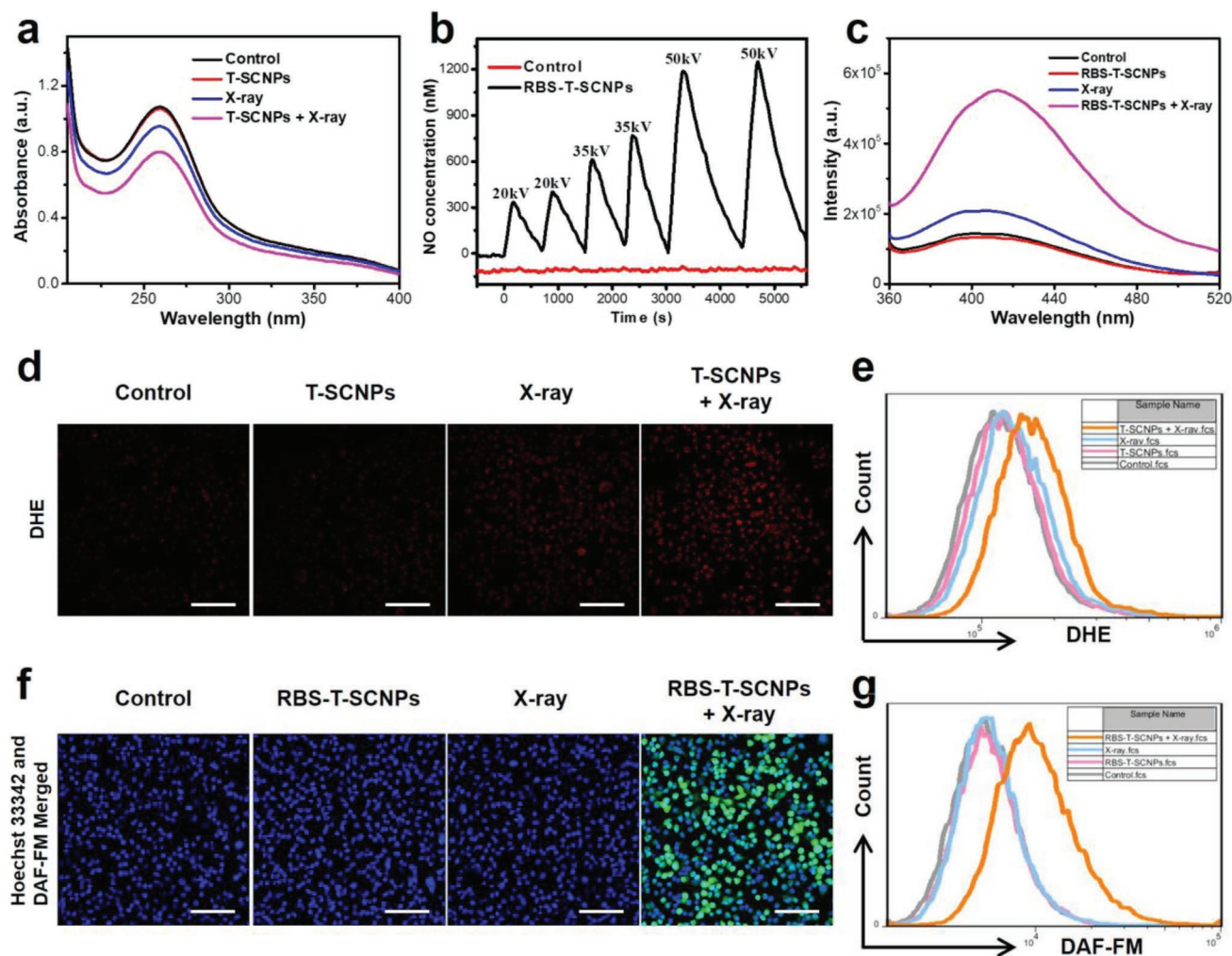
Figure 2. The measurements of X-ray-controlled $O_2^{-\bullet}$, NO, and $ONOO^-$ generation. a) The degradation of NBT by superoxide under different treatments. b) On/off behavior of the NO generation from RBS-T-SCNPs under diverse voltages of X-ray irradiation. c) Fluorescence of L-tyr in the system before and after adding RBS-T-SCNPs and illuminated with X-ray for 10 min. d) Fluorescence images for A549 cells staining with DHE (a superoxide fluorescent probe, red) with different treatments. The scale bar is 100 µm. e) Flow cytometry fluorescence histogram of DHE intensity in A549 cells with different treatments. f) Fluorescence images for A549 cells staining with Hoechst 33 342 (blue) and DAF-FM (a NO fluorescent probe, green) upon being treated with PBS or RBS-T-SCNPs in dark condition or under X-ray irradiation. The scale bar is 100 µm. g) Flow cytometry fluorescence histogram of DAF-FM intensity in A549 cells with different treatments.

in situ when being treated with T-SCNPs under X-ray irradiation (Figure 2). Then, the intracellular NO generation was monitored by a commercial NO fluorescence indicator, 3-amino-4-aminomethyl-2′,7′-difluorescein, diacetate (DAF-FM DA). As demonstrated in Figure 2f, a strong green fluorescence signal was observed only in the A549 cells treated with RBS-T-SCNPs + X-ray, indicating the radiation-responsive NO generation from RBS-T-SCNPs. The statistical data from flow cytometry in Figure 2g confirmed the above conclusion. These results verified that cellular NO and $O_2^{-\bullet}$ could be produced simultaneously under X-ray irradiation. Combined with the measurements in physiological solution, we can deduce that $ONOO^-$ was produced due to the close distance and rapid reaction between the simultaneously generated NO and $O_2^{-\bullet}$ under X-ray irradiation.

On the basis of the above results, we further investigated the radiotherapy efficiency of RBS-T-SCNPs in vitro. First,

the cytotoxicity was evaluated by CCK-8 assay and calcein AM/propidium iodide (CA-PI) double staining on both A549 cells and human umbilical vein endothelial cells. The results showed the low cytotoxicity of both T-SCNPs and RBS-T-SCNPs (Figures S10 and S11, Supporting Information). Next, the time-dependent cellular uptake of RBS-T-SCNPs was observed in A549 cells through dark-field microscopy, and the results from inductively coupled plasma-mass spectrometry showed that SCNPs could enter into cells rapidly within 6 h (Figures S12 and S13, Supporting Information). Then, the clonogenic survival assay was performed to evaluate the radiotherapy enhancement efficacy of RBS-T-SCNPs. As shown in **Figure 3**a,b, X-ray treatments decreased A549 cell colony formation to 52.1%, while T-SCNPs + X-ray treatment reduced cell survival to 36.4%, indicating the promising potential of T-SCNPs as the physical sensitizers for radiotherapy. More
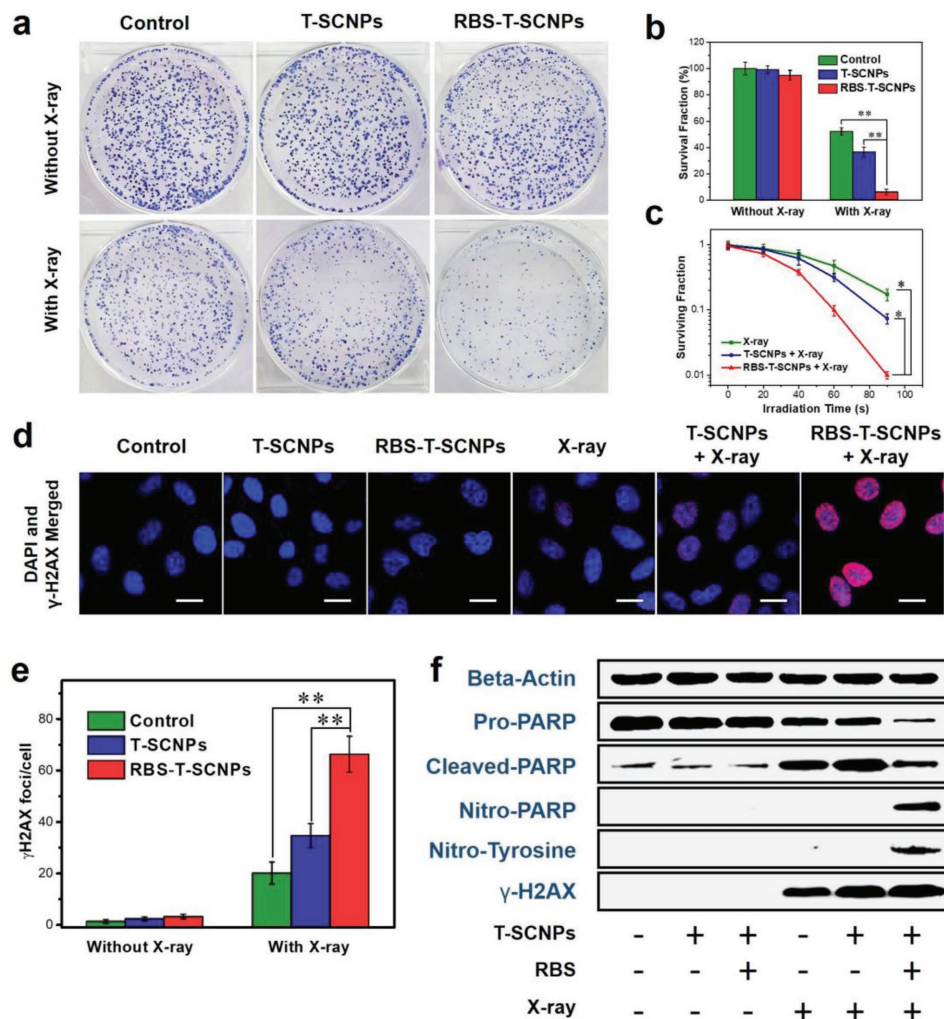
Figure 3. The radiosensitization efficiency of RBS-T-SCNPs in vitro. a) Colony formation assay of A549 cells incubated with T-SCNPs or RBS-T-SCNPs with or without X-ray irradiation. b) The corresponding surviving fraction of A549 cells with various treatments. c) The cell survival curves as a function of radiation doses detected by colony formation assay. d) Representative γ-H2AX immunofluorescence images with different treatments. The scale bar is 20 μm. e) Corresponding normalized number of γ-H2AX with different treatments. f) Western blot for the detection of Pro-PARP, Cleaved-PARP, Nitro-PARP, Nitro-Tyrosine, and γ-H2AX expression in A549 cells with different treatments. The error bars represent standard deviation for $n = 3$, P values were based on the Student's t-test: *$P < 0.01$, **$P < 0.001$.

importantly, the RBS-T-SCNPs + X-ray group showed only 5.9% cell survival. Additionally, the cell survival curves as a function of radiation doses were shown in Figure 3c and the sensitizer enhancement ratio (SER) was also calculated to assess the radiosensitization efficiency. The SER of RBS-T-SCNPs + X-ray group was about 1.81, which was significantly higher than that of X-ray treated only group, indicating the enhancement of therapeutic effect by RBS-T-SCNPs. Furthermore, similar radiosensitization efficiency was also observed in human hepatocellular carcinoma (BEL-7402) cells (Figures S14 and S15, Supporting Information). Next, the apoptosis/necrosis of A549 cells after different treatment was evaluated by Annexin V-FITC/PI staining (Figure S16, Supporting Information). The results showed that the T-SCNPs + X-ray treatment caused more cells' death than X-ray treatment because of the strong X-ray absorbing capability of the high-Z elements and more ROS generation from SCNPs under X-ray irradiation (Figures S17

and S18, Supporting Information). Interestingly, the $O_2^{-\bullet}$ produced from SCNPs and NO generated from RBS could quickly form $ONOO^-$ upon X-ray irradiation, making RBS-T-SCNPs effective radiosensitizers. Besides, the ineffective RBS-T-SCNPs treatment further confirmed that no premature formation of $ONOO^-$ under actual physiological conditions, explaining that the release of $ONOO^-$ could only be triggered by X-ray irradiation. From the above results, we can deduce that the sufficient generation of $ONOO^-$ by RBS-T-SCNPs under X-ray irradiation has a great potential in enhancing the radiotherapy efficiency.

To further investigate the radiosensitization mechanism of $ONOO^-$ from RBS-T-SCNPs, the DNA damage and the expression of several relevant proteins were detected. It is generally acknowledged that the radiation injury was attributed to the DNA damage, which was usually marked by the Phospho-Histone H2A.X (γ-H2AX, phosphorylation at serine 139).[20] Therefore, the cellular γ-H2AX expression was first

confirmed by the immunofluorescence staining. As shown in Figure 3d, the fluorescence intensities of γ-H2AX antibody in all the six groups were consistent with the cell colony assay results. In contrast to X-ray group, an increased fluorescence could be observed in T-SCNPs + X-ray group, which demonstrated the augment of DNA damage by T-SCNPs in radiotherapy. More importantly, the maximum production of DNA damage was observed in RBS-T-SCNPs + X-ray group. The corresponding statistic results were displayed in Figure 3e. It was suggested that RBS-T-SCNPs could greatly increase the DNA damage induced by X-ray and thus inhibit the proliferation of cancer cells. In most cases, the DNA damage induced by ionizing radiation would be rapidly repaired by poly(ADP-ribose) poerase (PARP), which is an abundant nuclear enzyme that promotes the repair of damaged DNA by binding to sites of the DNA strand breaks.[21] Therefore, the inhibition of PARP became an effective approach to fix DNA damage and cause cells' death.[22] Interestingly, growing evidence suggested that ONOO⁻ was a potent PARP inhibitor by the direct targeting of the zinc-finger motifs on PARP proteins.[23] Therefore, the influence of RBS-T-SCNPs and X-ray on the function of PARP was evaluated by western blotting. As presented in Figure 3f, the expression of Pro-PARP and Cleaved-PARP kept stable in the groups treated with T-SCNPs and RBS-T-SCNPs. However, the expression level of Pro-PARP reduced remarkably under X-ray irradiation, especially in the RBS-T-SCNPs + X-ray group. The decreased expression of Pro-PARP indicated the lack of DNA-repair ability in tumor cells. It could explain the reason why RBS-T-SCNPs caused more serious DNA damage during radiotherapy. At the same time, the expression of Cleaved-PARP increased in the groups with X-ray irradiation. In most cases, Pro-PARP could be cleaved by caspase family to form Cleaved-PARP after the activation of apoptosis. It is noteworthy that the expression levels of both Pro-PARP and Cleaved-PARP in RBS-SCNP + X-ray group were much lower than those in T-SCNPs + X-ray group. We speculated that these abnormal changes of Pro-PARP and Cleaved-PARP in RBS-SCNP + X-ray group might attribute to the nitration of the PARP proteins by ONOO⁻. To prove our hypothesis, the expressions of Nitro-PARP and Nitro-Tyrosine were detected. The results showed that the Nitro-PARP was considerably highly expressed in RBS-T-SCNPs + X-ray group while there was almost no expression in other groups. Additionally, the generation of ONOO⁻ was further confirmed by the expression of Nitro-Tyrosine, which is a clinical marker of ONOO⁻.[1b,4b] As shown in Figure 3f, Nitro-Tyrosine was only expressed in RBS-T-SCNPs + X-ray group, demonstrating the effective generation of ONOO⁻ by RBS-T-SCNPs under X-ray irradiation. From these results, we could draw a primary conclusion that the radiation-induced DNA damage was increased in the presence of high-Z SCNPs, but the PARP-associated DNA-repair process could also be activated accordingly, which might reduce the radiotherapy efficiency in tumor cells. While RBS-T-SCNPs could produce ONOO⁻ upon X-ray irradiation, which caused the nitration of PARP protein and the fixation of DNA damage, ultimately promoting cell death.

Besides the DNA-repair ability of PARP that limited the radiotherapy efficiency, tumor hypoxia is another key factor that contributed to the observed radioresistance and subsequent recurrence of tumors.[24] Furthermore, traditional radiotherapy might exacerbate the hypoxic microenvironment, causing even less injury of tumor cells. As we know, NO can serve as an effective vasodilator to improve the blood circulation and tumor oxygenation, which makes it a hypoxic radiosensitizer.[25] The vascular saturated O_2 within A549 solid tumors was evaluated by the following photoacoustic (PA) imaging. After being treated with RBS-T-SCNPs and X-ray irradiation, the tumor hypoxia status was monitored by the PA signals of deoxygenated (blue) and oxygenated (red) hemoglobin (Figure S19, Supporting Information). The intratumoral injection of RBS-T-SCNPs did not affect the signals of deoxygenated and oxygenated hemoglobin in tumors. However, after the X-ray irradiation, both the signals of deoxygenated and oxygenated hemoglobin were significantly enhanced. This result suggested that NO from RBS-T-SCNPs indeed dilated the blood vessels and consequently enhanced tumor oxygenation. As tumor hypoxia played an important role in radiotherapy, RBS-T-SCNPs have great potential to be an effective radiosensitizer to overcome hypoxia-induced radiotherapy resistance.

Encouraged by the successful effects on inhibiting the DNA repairing and overcoming tumor hypoxia, we further evaluated the enhanced radiotherapy sensitization of RBS-T-SCNPs in vivo. The A549-tumor-bearing Balb/c mice were randomly divided into six groups (control, T-SCNPs, RBS-T-SCNPs, X-ray, T-SCNPs + X-ray, RBS-T-SCNPs + X-ray). T-SCNPs and RBS-T-SCNPs were intratumorally injected, followed by the irradiation treatment (6 Gy). As shown in **Figure 4**a,b, the relative tumor volumes and tumor weights have no significant difference in control, T-SCNPs, and RBS-T-SCNPs (nonirradiated) groups, confirming no significant toxicity of these nanomaterials. However, the obvious inhibitions of tumor growth appeared in all the irradiated groups, especially in RBS-T-SCNPs + X-ray group. Furthermore, hematoxylin and eosin (H&E) staining of tumors in Figure 4c also revealed that RBS-T-SCNPs + X-ray group exhibited the most severe cancer cells tumor tissue damage, while only X-ray radiation could not induce such damage on tumor tissue, further validating the enhanced radiotherapy efficiency of RBS-T-SCNPs.

To further investigate the radiosensitization mechanism of RBS-T-SCNPs, tumor slices collected from different groups were analyzed by immunohistochemistry (Figure 4c). First, we confirmed the generation of ONOO⁻ in the RBS-T-SCNPs + X-ray group through detecting the expression of Nitro-Tyrosine. Then, the levels of DNA damage and DNA repair were demonstrated by the expression of γ-H2AX and Cleaved-PARP, respectively. The results showed more DNA damages in RBS-T-SCNPs + X-ray group than the other X-ray treated groups. At the same time, the expression level of Cleaved-PARP increased remarkably in both of X-ray group and T-SCNPs + X-ray group, indicating the apparent DNA repairing in these groups. However, after RBS-T-SCNPs and X-ray treatment, the expression level of Cleaved-PARP kept stable compared with the control group. These results clearly illustrated that the X-ray-induced ONOO⁻ from RBS-T-SCNPs could inhibit the function of DNA-repair enzyme and further aggravate DNA damage. Besides, the expression of hypoxia inducible factor-1α (HIF-1α) decreased significantly in the RBS-T-SCNPs + X-ray group. Since HIF-1α was considered as a marker of tumor hypoxia, the obvious
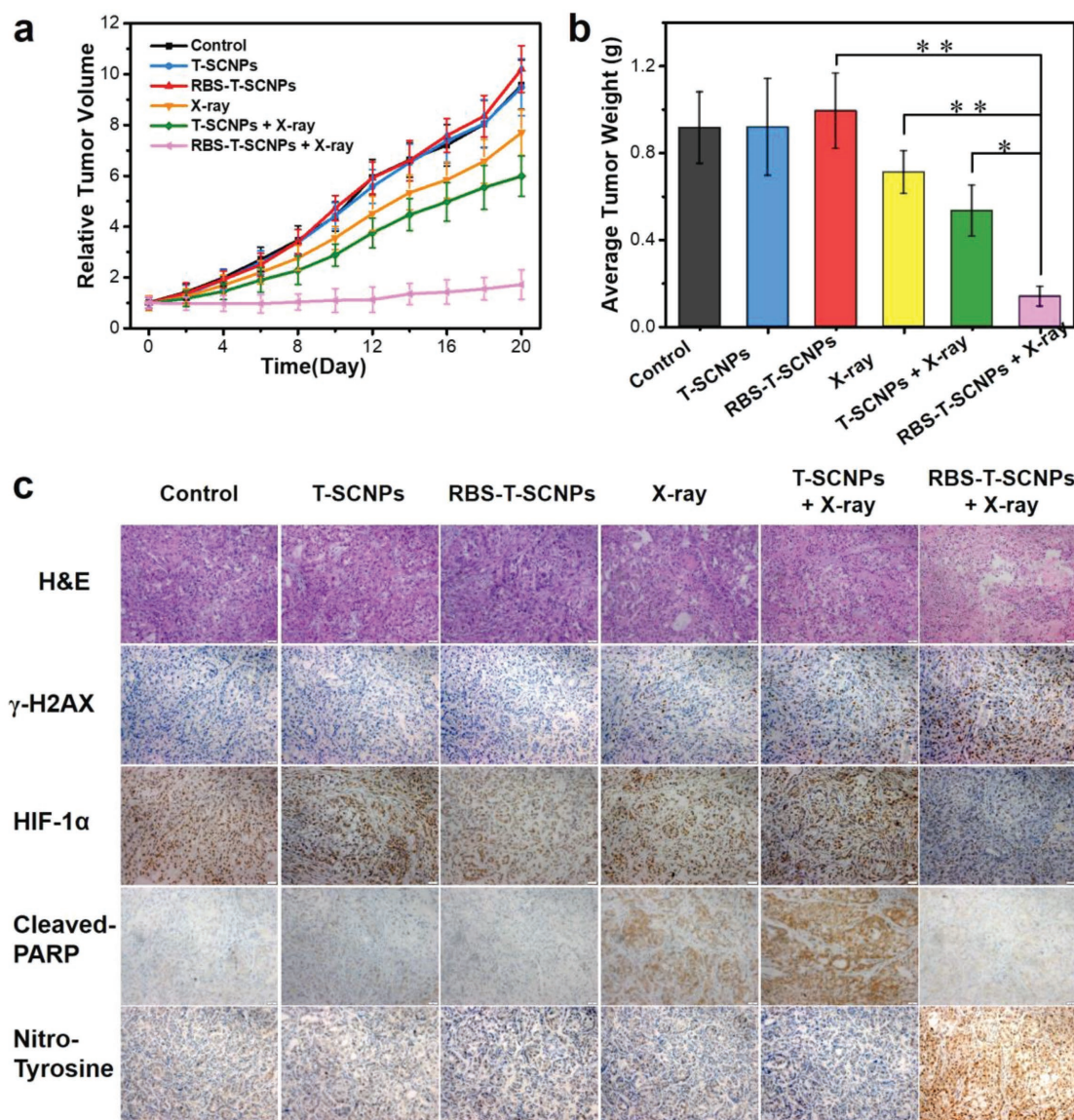
Figure 4. In vivo antitumor efficacy of A549-tumor-bearing nude mice. a) Relative tumor volume curves of different groups of mice after different treatments: i) PBS; ii) T-SCNPs; iii) RBS-T-SCNPs; iv) X-ray; v) T-SCNPs + X-ray; vi) RBS-T-SCNPs + X-ray. b) Tumor weights of different groups of mice 20 d after different treatments. c) Representative H&E stained images and immunohistochemical analysis of tumor slices collected from various groups of mice. Error bars represent standard deviation for $n = 4$, P values were based on the Student's t-test: *$P < 0.01$, **$P < 0.001$.

downregulation of HIF-1α implied the relief of hypoxia status in the RBS-T-SCNPs + X-ray group. Taken together, these reactive nitrogen species (including ONOO$^-$ and NO) could not only inhibit the repair of the damaged DNA by means of deactivating DNA-repair enzymes but also relieve hypoxia within tumors. In addition, the body weight in each group had no significant differences while no apparent abnormality in the major organs was observed (Figures S20–S24, Supporting Information). The significant parameters of the blood hematology and biochemistry analyses also showed no noticeable changes (Figures S25 and S26, Supporting Information). In consideration of the strong X-ray attenuation capability, SCNPs were also anticipated to be the contrast agents in CT image (Figures S27 and S28, Supporting Information). Furthermore, the radioluminescence property of SCNPs leading to the

potential use in X-ray luminescence optical tomography applications.[26] All of the above results proved the good biocompatibility and effective radiosensitization of RBS-T-SCNPs, which possess the remarkable potential in X-ray-controlled ONOO$^-$ generation as well as cancer diagnosis and treatment.

In summary, we developed a nanocomposite containing SCNPs and RBS for X-ray-induced ONOO$^-$ generation and applications in radiosensitization. On the basis of the simultaneous generation of O$_2^{-\cdot}$ from SCNPs and NO from RBS, X-ray-triggered ONOO$^-$ release could be achieved in vitro and in vivo. The generated ONOO$^-$ effectively inhibited the PARP-associated DNA-repair process, leading to the augment of DNA damage and the sensitization of radiotherapy. Meanwhile, the controlled generation of ONOO$^-$ and NO significantly reduced hypoxia in tumors, which could overcome the hypoxia-associated resistance

**ADVANCED
SCIENCE NEWS**

www.advancedsciencenews.com

**ADVANCED
MATERIALS**

www.advmat.de

in radiotherapy. Additionally, the imaging capability of SCNPs may offer an additional method for diagnostic application. These findings demonstrate the great potential of RBS-T-SCNPs for effective theranostic agents in cancer radiotherapy.

Supporting Information

Acknowledgements

Conflict of Interest

The authors declare no conflict of interest.

Keywords

[1] a) P. Pacher, J. S. Beckman, L. Liaudet, *Physiol. Rev.* **2007**, *87*, 315; b) G. Ferrer-Sueta, N. Campolo, M. Trujillo, S. Bartesaghi, S. Carballal, N. Romero, B. Alvarez, R. Radi, *Chem. Rev.* **2018**, *118*, 1338.

[2] a) D. D. Thomas, X. Liu, S. P. Kantrow, J. R. Lancaster, *Proc. Natl. Acad. Sci. USA* **2001**, *98*, 355; b) I. Fridovich, *J. Biol. Chem.* **1997**, *272*, 18515.

[3] a) H. Botti, M. N. Möller, D. Steinmann, T. Nauser, W. H. Koppenol, A. Denicola, R. Radi, *J. Phys. Chem. B* **2010**, *114*, 16584; b) J. S. Beckman, W. H. Koppenol, *Am. J. Physiol.* **1996**, *271*, C1424.

[4] a) J. S. Beckman, T. W. Beckman, J. Chen, P. A. Marshall, B. A. Freeman, *Proc. Natl. Acad. Sci. USA* **1990**, *87*, 1620; b) J. S. Beckman, *Ann. N. Y. Acad. Sci.* **1994**, *738*, 69.

[5] a) L. Virag, E. Szabo, P. Gergely, C. Szabo, *Toxicol. Lett.* **2003**, *140–141*, 113; b) D. Wang, L. Niu, Z. Y. Qiao, D. B. Cheng, J. Wang, Y. Zhong, F. Bai, H. Wang, H. Fan, *ACS Nano* **2018**, *12*, 3796; c) C. Szabo, *Toxicol. Lett.* **2003**, *140–141*, 105; d) R. Radi, J. S. Beckman, K. M. Bush, B. A. Freeman, *Arch. Biochem. Biophys.* **1991**, *288*, 481.

[6] L. Zhu, V. P. Torchilin, *Integr. Biol.* **2013**, *5*, 96.

[7] a) S. Sortino, *Chem. Soc. Rev.* **2010**, *39*, 2903; b) X. Zhang, G. Tian, W. Y. Yin, L. M. Wang, X. P. Zheng, L. Yan, J. X. Li, H. R. Su, C. Y. Chen, Z. J. Gu, Y. L. Zhao, *Adv. Funct. Mater.* **2015**, *25*, 3049; c) X. Zhang, Z. Guo, J. Liu, G. Tian, K. Chen, S. Yu, Z. Gu, *Sci. Bull.* **2017**, *62*, 985.

[8] a) C. Zhang, K. Zhao, W. Bu, D. Ni, Y. Liu, J. Feng, J. Shi, *Angew. Chem.* **2015**, *54*, 1770; b) H. Chen, G. D. Wang, Y. J. Chuang, Z. Zhen, X. Chen, P. Biddinger, Z. Hao, F. Liu, B. Shen, Z. Pan, J. Xie, *Nano Lett.* **2015**, *15*, 2249; c) A. Kamkaew, F. Chen, Y. Zhan,

R. L. Majewski, W. Cai, *ACS Nano* **2016**, *10*, 3918; d) C. L. Melcher, J. S. Schweitzer, *IEEE Trans. Nucl. Sci.* **1992**, *39*, 502.

[9] a) D. Schaue, W. H. McBride, *Nat. Rev. Clin. Oncol.* **2015**, *12*, 527; b) A. C. Begg, F. A. Stewart, C. Vens, *Nat. Rev. Cancer* **2011**,*11*, 239.

[10] a) H. Wang, X. Mu, H. He, X. D. Zhang, *Trends Pharmacol. Sci.* **2018**, *39*, 24; b) S. Klein, C. Harreiss, C. Menter, J. Hummer, L. V. R. Distel, K. Meyer, R. Hock, C. Kryschi, *ACS Appl. Mater. Interfaces* **2018**, *10*, 17071.

[11] a) D. Kwatra, A. Venugopal, S. Anant, *Transl. Cancer Res.* **2013**, *2*, 330; b) P. Retif, S. Pinel, M. Toussaint, C. Frochot, R. Chouikrat, T. Bastogne, M. Barberi-Heyob, *Theranostics* **2015**, *5*, 1030; c) G. Song, L. Cheng, Y. Chao, K. Yang, Z. Liu, *Adv. Mater.* **2017**, *29*, 1700996.

[12] F. H. Agani, M. Puchowicz, J. C. Chavez, P. Pichiule, J. LaManna, *Am. J. Physiol. Cell Physiol.* **2002**, *283*, C178.

[13] P. Huang, W. Zheng, S. Zhou, D. Tu, Z. Chen, H. Zhu, R. Li, E. Ma, M. Huang, X. Chen, *Angew. Chem., Int. Ed.* **2014**, *53*, 1252.

[14] a) T. Yanagida, Y. Fujimoto, N. Kawaguchi, Y. Yokota, K. Kamada, D. Totsuka, S. I. Hatamoto, A. Yoshikawa, V. Chani, *Nucl. Instrum. Methods Phys. Res., Sect. A* **2011**, *652*, 251; b) C. M. Combes, P. Dorenbos, C. W. E. vanEijk, C. Pedrini, H. W. DenHartog, J. Y. Gesland, P. A. Rodnyi, *J. Lumin.* **1997**, *71*, 65.

[15] N. Bogdan, F. Vetrone, G. A. Ozin, J. A. Capobianco, *Nano Lett.* **2011**, *11*, 835.

[16] a) G. Tian, X. Zheng, X. Zhang, W. Yin, J. Yu, D. Wang, Z. Zhang, X. Yang, Z. Gu, Y. Zhao, *Biomaterials* **2015**, *40*, 107; b) J. M. Dintaman, J. A. Silverman, *Pharm. Res.* **1999**, *16*, 1550; c) Z. Zhang, S. Tan, S. S. Feng, *Biomaterials* **2012**, *33*, 4889.

[17] J. Bourassa, W. DeGraff, S. Kudo, D. A. Wink, J. B. Mitchell, P. C. Ford, *J. Am. Chem. Soc.* **1997**, *119*, 2853.

[18] S. Obregon, M. A. Ruiz-Gomez, D. B. Hernandez-Uresti, *J. Colloid Interface Sci.* **2017**, *506*, 111.

[19] a) M. Misawa, J. Takahashi, *Nanomedicine* **2011**, *7*, 604; b) S. Her, D. A. Jaffray, C. Allen, *Adv. Drug. Deliv. Rev.* **2017**, *109*, 84.

[20] E. P. Rogakou, D. R. Pilch, A. H. Orr, V. S. Ivanova, W. M. Bonner, *J. Biol. Chem.* **1998**, *273*, 5858.

[21] A. A. Pieper, A. Verma, J. Zhang, S. H. Snyder, *Trends Pharmacol. Sci.* **1999**, *20*, 171.

[22] a) A. Sonnenblick, E. de Azambuja, H. A. Azim Jr., M. Piccart, *Nat. Rev. Clin. Oncol.* **2015**, *12*, 27; b) Q. Liu, L. Gheorghiu, M. Drumm, R. Clayman, A. Eidelman, M. F. Wszolek, A. Olumi, A. Feldman, M. Wang, L. Marcar, D. E. Citrin, C. L. Wu, C. H. Benes, J. A. Efstathiou, H. Willers, *Oncogene* **2018**, *37*, 2793; c) C. R. Calabrese, R. Almassy, S. Barton, M. A. Batey, A. H. Calvert, S. Canan-Koch, B. W. Durkacz, Z. Hostomsky, R. A. Kumpf, S. Kyle, J. Li, K. Maegley, D. R. Newell, E. Notarianni, I. J. Stratford, D. Skalitzky, H. D. Thomas, L. Z. Wang, S. E. Webber, K. J. Williams, N. J. Curtin, *J. Natl. Cancer Inst.* **2004**, *96*, 56; d) L. Virag, C. Szabo, *Pharmacol. Rev.* **2002**, *54*, 375.

[23] O. Sidorkina, M. G. Espey, K. M. Miranda, D. A. Wink, J. Laval, *Free Radicals Biol. Med.* **2003**, *35*, 1431.

[24] a) Y. Yong, C. Zhang, Z. Gu, J. Du, Z. Guo, X. Dong, J. Xie, G. Zhang, X. Liu, Y. Zhao, *ACS Nano* **2017**, *11*, 7164; b) J. Kim, H. R. Cho, H. Jeon, D. Kim, C. Song, N. Lee, S. H. Choi, T. Hyeon, *J. Am. Chem. Soc.* **2017**, *139*, 10992; c) M. Hockel, K. Schlenger, B. Aral, M. Mitze, U. Schaffer, P. Vaupel, *Cancer Res.* **1996**, *56*, 4509; d) J. M. Brown, W. R. Wilson, *Nat. Rev. Cancer* **2004**, *4*, 437.

[25] a) M. De Ridder, D. Verellen, V. Verovski, G. Storme, *Nitric Oxide* **2008**, *19*, 164; b) W. Fan, W. Bu, Z. Zhang, B. Shen, H. Zhang, Q. He, D. Ni, Z. Cui, K. Zhao, J. Bu, J. Du, J. Liu, J. Shi, *Angew. Chem.* **2015**, *54*, 14026; c) Z. Du, R. Dou, M. Zu, X. Liu, W. Yin, Y. Zhao, J. Chen, L. Yan, Z. Gu, *Biomater. Sci.* **2016**, *4*, 938; d) R. M. Palmer, A. G. Ferrige, S. Moncada, *Nature* **1987**, *327*, 524.

[26] a) L. Sudheendra, G. K. Das, C. Li, D. Stark, J. Cena, S. Cherry, I. M. Kennedy, *Chem. Mater.* **2014**, *26*, 1881; b) P. Lecoq, *Nucl. Instrum. Methods Phys. Res., Sect. A* **2016**, *809*, 130.